Journal of Cosmology and Astroparticle Physics
An IOP and SISSA journal

On the validity of the effective field theory for dark matter searches at the LHC part III: analysis for the t-channel

Giorgio Busoni,[a] **Andrea De Simone,**[a] **Thomas Jacques,**[b] **Enrico Morgante**[b] **and Antonio Riotto**[b]

[a]SISSA and INFN, Sezione di Trieste,
via Bonomea 265, I-34136 Trieste, Italy
[b]Section de Physique, Université de Genève,
24 quai E. Ansermet, CH-1211 Geneva, Switzerland

E-mail: giorgio.busoni@sissa.it, andrea.desimone@sissa.it, thomas.jacques@unige.ch, enrico.morgante@unige.ch, antonio.riotto@unige.ch

Received July 8, 2014
Revised August 8, 2014
Accepted August 13, 2014
Published September 10, 2014

Abstract. We extend our recent analysis of the limitations of the effective field theory approach to studying dark matter at the LHC, by investigating the case in which Dirac dark matter couples to standard model quarks via t-channel exchange of a heavy scalar mediator. We provide analytical results for the validity of the effective field theory description, for both $\sqrt{s} = 8\,\text{TeV}$ and $14\,\text{TeV}$. We make use of a MonteCarlo event generator to assess the validity of our analytical conclusions. We also point out the general trend that in the regions where the effective field theory is valid, the dark matter relic abundance is typically large.

Keywords: dark matter theory, dark matter experiments

ArXiv ePrint: 1405.3101

doi:10.1088/1475-7516/2014/09/022

JCAP09(2014)022

Contents

1 Introduction 1

2 Validity of the EFT: analytical approach 3
- 2.1 Operators and cross sections 3
- 2.2 Results and discussion 5
- 2.3 Comparison with MonteCarlo simulations 8

3 Conclusions 8

A Three-body cross sections 9
- A.1 Matrix elements 10
- A.2 Cross sections 11
- A.3 Transferred momentum 13

1 Introduction

Despite overwhelming gravitational evidence for the existence of dark matter (DM), we still have very little information about its particle properties. Yet there is enough evidence to motivate a search for DM with a mass at the electroweak energy scale, with non-zero albeit very weak interactions with the Standard Model (SM), known as a weakly interacting massive particle (WIMP). Both direct and indirect detection have been very successful at placing strong, model independent constraints on the WIMP-nucleon scattering rate and self-annihilation rate respectively [1–7], and whilst there are anomalies that may be consistent with a WIMP signal [8–10], a conclusive discovery has not been achieved.

The LHC is searching for direct DM production at unprecedented energies, and has excellent potential to finally discover DM. Mono-jet [11–14], mono-W/Z [15, 16] and mono-photon [17–20] searches are currently under way to look for an indirect signature of DM production. Yet, given that the true nature of DM is unknown, it has proven difficult to constrain the WIMP sector as a whole in a model-independent way. One potential solution to this problem is the use of Effective Field Theories (EFTs), which allow a DM-SM interaction term to be written as a single effective operator, integrating out the mediator.[1] This has the advantage of reducing the parameter space to a single energy scale, Λ (sometimes called M_* in the literature), in addition to the DM mass, and reducing the potential number of WIMP models down to a relatively small basis set.

EFTs are inherently an approximation to a full UV-complete theory, and hence must be used with caution. Given that the LHC is operating at very large energies, it is important to ensure that constraints on EFTs are internally consistent and fall in a region where the EFT approximation is valid.

This issue has been investigated in refs. [23, 24] where the validity of the EFT at both $\sqrt{s}$ =8 and 14 TeV has been tested when heavy mediators are exchanged in the s-channel. In particular, the validity of the EFT was assessed by introducing a few quantities, some of them independent of the ultraviolet completion of the DM theory, which quantify the

[1] See e.g. refs. [21, 22] for recently proposed directions alternative to EFT and simplified models for DM searches at the LHC.

JCAP09(2014)022

error made when using effective operators to describe processes with very high momentum transfer. It was found that only a small fraction of events were at energies where the EFT approximation is valid, regardless of the choice of cuts or operator. In addition, refs. [25, 26] have compared constraints on some EFTs to those on simplified models where the mediator has not been integrated out, and found that constraints on Λ using UV complete models can either be substantially stronger or substantially weaker than those constructed using EFTs, depending on the choice of parameters. Since the initial motivation of using EFTs is to place model independent constraints on the dark sector independent of assumptions about the input parameters, it is becoming clear that extreme caution must be used when placing constraints on DM using EFTs at the LHC.

In this paper we extend the analysis of refs. [23, 24] to the t-channel. We consider a model where Dirac DM couples to SM quarks via t-channel exchange of a scalar mediator. The details of the model are described in section 2. Our goal is to determine in what regions of parameter space the EFT approach is a valid description of this model. The EFT approximation is made by integrating out the mediator particle, and combining the mediator mass M with the coupling strength g into a single energy scale, $\Lambda \equiv M/g$. This is done by expanding the propagator term for the mediator in powers of $Q_{\rm tr}^2/M^2$ and truncating at the lowest order, where $Q_{\rm tr}$ is the momentum carried by the mediator:

$$\frac{g^2}{Q_{\rm tr}^2 - M^2} = -\frac{g^2}{M^2}\left(1 + \frac{Q_{\rm tr}^2}{M^2} + \mathcal{O}\left(\frac{Q_{\rm tr}^4}{M^4}\right)\right) \tag{1.1}$$

$$\simeq -\frac{1}{\Lambda^2}. \tag{1.2}$$

Clearly, this approximation is only valid when $Q_{\rm tr}^2 \ll M^2$; yet this condition is impossible to test precisely in the true EFT limit, since M has been combined with g to form Λ. Instead, an assumption about g must be made, defeating one of the primary advantages of EFTs. This is unavoidable, since the LHC operates at energies high enough that violation of the EFT approximation is a real concern and must be tested, as has been seen in refs. [23, 24]. There is no lower limit to the unknown coupling strength g,[2] meaning that regardless of the scale of Λ, it is always possible that M is small enough that the EFT approximation does not apply, and the constraint on Λ is invalid. In other words, for all operators, constraints on Λ will only be valid down to a certain value of g if the EFT approach has been taken.

On the other hand, the most optimistic choice is to assume that $g \simeq 4\pi$, the maximum possible coupling strength such that the model still lies in the perturbative regime. This choice is discussed later in the text. As a middle ground, we test whether the EFT approximation is valid for values of $g \gtrsim 1$, a natural scale for the coupling in the absence of any other information. In this case, the condition for the validity of the EFT approximation becomes

$$Q_{\rm tr}^2 \lesssim \Lambda^2, \tag{1.3}$$

which we will adopt in the following to assess the validity of the use of EFT at LHC for DM searches.

The paper is organized as follows. Section 2 contains the bulk of our analytical results for both $\sqrt{s} = 8$ and 14 TeV and a comparison with those obtained using fully numerical simulations of the LHC events. Our discussion and conclusions are summarized in section 3.

[2] Although if g is particularly small, and the DM is a thermal relic, then DM will be overproduced in the early universe unless another annihilation channel is available.

JCAP09(2014)022

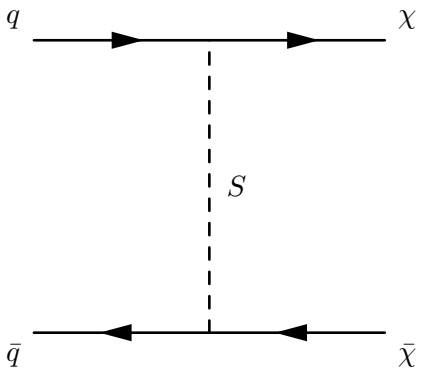

Figure 1. Illustrative $2 \to 2$ process for the UV-complete version of our effective operator.

2 Validity of the EFT: analytical approach

2.1 Operators and cross sections

In this paper we will consider the following effective operator describing the interactions between Dirac dark matter χ and left-handed quarks q

$$\mathcal{O} = \frac{1}{\Lambda^2} \left(\bar{\chi} P_L q\right) \left(\bar{q} P_R \chi\right). \tag{2.1}$$

Only the coupling between dark matter and the first generation of quarks is considered. Including couplings to the other generations of quarks requires fixing the relationships between the couplings and mediator masses for each generation, making such an analysis less general. In principle the dark matter can also couple to the right-handed quark singlet, switching P_R and P_L in the above operator. The inclusion of both of these operators does not modify our results, even if the two terms have different coupling strengths.

The operator in eq. (2.1) can be viewed as the low-energy limit of a simplified model describing a quark doublet Q_L coupling to DM, via t-channel exchange of a scalar mediator S_Q,

$$\mathcal{L}_{\rm int} = g\, \bar{\chi} Q_L S_Q^* + h.c. \tag{2.2}$$

and integrating out the mediator itself. Since we consider only coupling to the first generation of quarks, $Q_L = (u_L, d_L)$. As an illustration, the $2 \to 2$ process $q\bar{q} \to \chi\bar{\chi}$ for this model is shown in figure 1. This model is popular as an example of a simple DM model with t-channel couplings, which exist also in well-motivated models such as supersymmetry where the mediator particle is identified as a squark, and the DM is a Majorana particle. Bell et al. [27] have used a version of this model with Majorana DM in place of Dirac DM, to test the prospects of Z-bosons as a potential search channel. This has been followed up by a dedicated ATLAS search in this channel [16]. Refs. [28–33] have also constrained this model, using both the standard monojet search channel as well as searching for multiple jets arising from direct mediator production. Refs. [29, 33] found that collider constraints on this model were competitive if not stronger than direct detection constraints across most of the parameter space.

The t-channel operator in eq. (2.1) can be expressed as a sum of s-channel operators using Fierz transformations. For arbitrary Dirac spinors such as $\bar{q}_1$, q_2, $\bar{\chi}_1$, χ_2, and adopting

JCAP09(2014)022

in part the notation of [34], the Fierz transformation can be expressed as

$$(\bar{q}_1 X \chi_2)\,(\bar{\chi}_1 Y q_2) = \frac{1}{4}\sum_B \left(\bar{q}_1 X \Gamma^B Y q_2\right)\left(\bar{\chi}_1 \Gamma_B \chi_2\right), \tag{2.3}$$

where X, Y are some combination of Dirac-matrices, and $\Gamma^B = \{\mathbb{1}, i\gamma_5, \gamma^\mu, \gamma_5\gamma^\mu, \sigma^{\mu\nu}\}$ and $\Gamma_B = \{\mathbb{1}, -i\gamma_5, \gamma_\mu, -\gamma_5\gamma_\mu, \frac{1}{2}\sigma_{\mu\nu}\}$ form a basis spanning 4×4 matrices over the complex number field [34]. Due to the chiral coupling between the quarks and DM, most of the terms in the sum cancel, and we are left with

$$\begin{aligned}
\mathcal{O} &= \frac{1}{\Lambda^2}\left(\bar{\chi}P_L q\right)\left(\bar{q}P_R\chi\right) \\
&= \frac{1}{8\Lambda^2}\left(\bar{\chi}\gamma^\mu\chi\right)\left(\bar{q}\gamma_\mu q\right) && (D5)\\
&\quad + \frac{1}{8\Lambda^2}\left(\bar{\chi}\gamma^\mu\gamma_5\chi\right)\left(\bar{q}\gamma_\mu q\right) && (D6)\\
&\quad - \frac{1}{8\Lambda^2}\left(\bar{\chi}\gamma^\mu\chi\right)\left(\bar{q}\gamma_\mu\gamma_5 q\right) && (D7)\\
&\quad - \frac{1}{8\Lambda^2}\left(\bar{\chi}\gamma^\mu\gamma_5\chi\right)\left(\bar{q}\gamma_\mu\gamma_5 q\right) && (D8)\\
&= \frac{1}{2\Lambda^2}\left(\bar{\chi}\gamma^\mu P_R\chi\right)\left(\bar{q}\gamma_\mu P_L q\right).
\end{aligned} \tag{2.4}$$

This is equivalent to a rescaled sum of the $D5$, $D6$, $D7$ and $D8$ operators [35]. Thus, it is interesting to see whether the EFT limit of the t-channel model under investigation has similar phenomenology to these s-channel operators. This is discussed in section 3.

The standard search channel for such a scenario is missing energy ($\not{E}_T$) plus a single jet, although particles such as Z-bosons [16, 27] are promising complementary search channels. The dijet+$\not{E}_T$ channel is particularly promising for the simplified model in eq. (2.2) since direct production of a pair of mediator particles can result in a strong dijet signal. In particular, refs. [29, 32] found that in much of parameter space, the dijet signal from direct mediator production provides comparable or stronger constraints on the model than the traditional monojet signal. In the high-energy limit, the mediator particle has SM charges and can emit a gluon, photon or massive gauge boson. This channel is suppressed in the EFT limit and so is not considered here.

The dominant process contributing to the $\not{E}_T$+ monojet signal is $q\bar{q} \to \chi\bar{\chi}g$. Representations of the EFT diagrams are shown in figure 2. We have calculated the differential cross section for these processes, with the results given in appendix A along with the corresponding matrix elements. In the same appendix we have also calculated the differential cross section for the other contributing processes, $qg \to \chi\bar{\chi}q$ and $g\bar{q} \to \chi\bar{\chi}\bar{q}$, which we found to be subdominant. In the full simplified model, the scalar mediator carries standard model charges and can emit gauge bosons, including gluons which would contribute to the $\not{E}_T$+ monojet signal. This channel is neglected in this study, since we are testing whether the effective operator description of this model is internally consistent regardless of the UV completion.

In order to compute the cross section with proton initial states appropriate for LHC events, it is necessary to integrate over the parton distribution function (PDF) of the proton. For $q\bar{q}$ initial states, this is defined as

$$\sigma = \sum_q \int \mathrm{d}x_1 \mathrm{d}x_2 [f_q(x_1) f_{\bar{q}}(x_2) + f_q(x_2) f_{\bar{q}}(x_1)]\hat{\sigma}, \tag{2.5}$$

JCAP09(2014)022

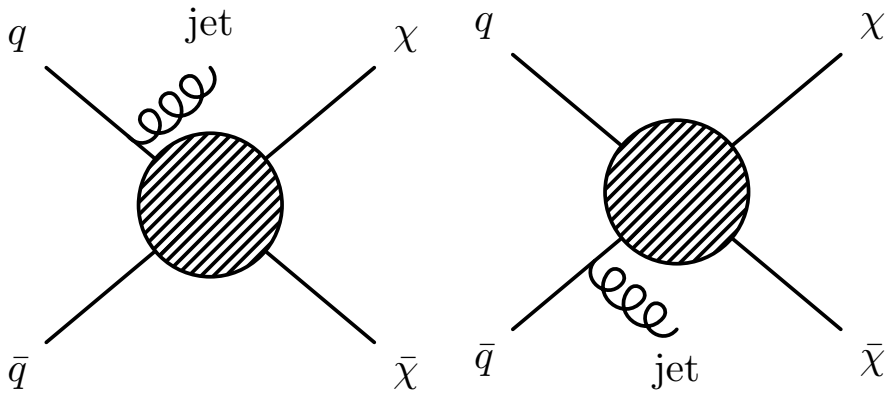

Figure 2. Search channel.

where $\hat{\sigma}$ is the total cross section for a process in the center of momentum frame. We have used the MSTW PDFs from refs. [36, 37], and checked that the our results are not sensitive to the choice of leading or next-to-leading-order MSTW PDFs.

2.2 Results and discussion

Recall that our goal is to determine whether the EFT approximation is valid for the operator in eq. (2.1), in the standard search channel $q\bar{q} \to \chi\bar{\chi}+$ jet, when the coupling strength is at roughly the natural scale, $1 \lesssim g \lesssim 4\pi$. In this case, for any given event, the momentum of the mediator can only be neglected if $Q_{\rm tr}^2 \lesssim \Lambda^2$. To test this, we define the ratio of the cross section truncated so that all events pass the condition, to the total cross section:

$$R_\Lambda \equiv \frac{\sigma|_{Q_{\rm tr}<\Lambda}}{\sigma} = \frac{\int_{p_{\rm T}^{\rm min}}^{p_{\rm T}^{\rm max}} {\rm d}p_{\rm T} \int_{-2}^{2} {\rm d}\eta \left.\frac{{\rm d}^2\sigma}{{\rm d}p_{\rm T}{\rm d}\eta}\right|_{Q_{\rm tr}<\Lambda}}{\int_{p_{\rm T}^{\rm min}}^{p_{\rm T}^{\rm max}} {\rm d}p_{\rm T} \int_{-2}^{2} {\rm d}\eta \frac{{\rm d}^2\sigma}{{\rm d}p_{\rm T}{\rm d}\eta}}. \tag{2.6}$$

We have parameterised the cross section such that the final integration variables are the standard observables for jets observed at the LHC, namely the transverse momentum $p_{\rm T}$ and pseudorapidity η. The integration limits on these quantities are chosen to be comparable to those used in standard searches for WIMP DM by the LHC collaborations (see, for instance, ref. [13]). For searches at center of mass energy $\sqrt{s} = 8\,{\rm TeV}$, $p_{\rm T}$ is integrated from 500 GeV to 1 TeV. For $\sqrt{s} = 14\,{\rm TeV}$, the integration range is instead 500 GeV to 2 TeV. In both cases, the pseudorapidity integration range is $|\eta| \leq 2$.

There are two values of $Q_{\rm tr}$, corresponding to jet emission from either the initial state quark or antiquark respectively. These are given in appendix A.3. Mixing between diagrams makes it impossible to disentangle a single transferred momentum for any individual event, and so we require that for each event *both* values of $Q_{\rm tr}$ for that process satisfy the requirement that $Q_{\rm tr}^2 < \Lambda^2$.

In figure 3 we show the behaviour of R_Λ as a function of Λ, at both $\sqrt{s}$ =8 and 14 TeV. Similarly, figure 4 shows R_Λ as a function of $m_{\rm DM}$ at the same center of mass energies. In figure 5 we instead plot isocontours of four fixed values of R_Λ as a function of both $m_{\rm DM}$ and Λ. Contrasted with the s-channel case [23, 24], the ratio has less DM mass dependence, being even smaller than in the s-channel case at low DM masses and larger at large DM masses, without becoming large enough to save EFTs.

JCAP09(2014)022

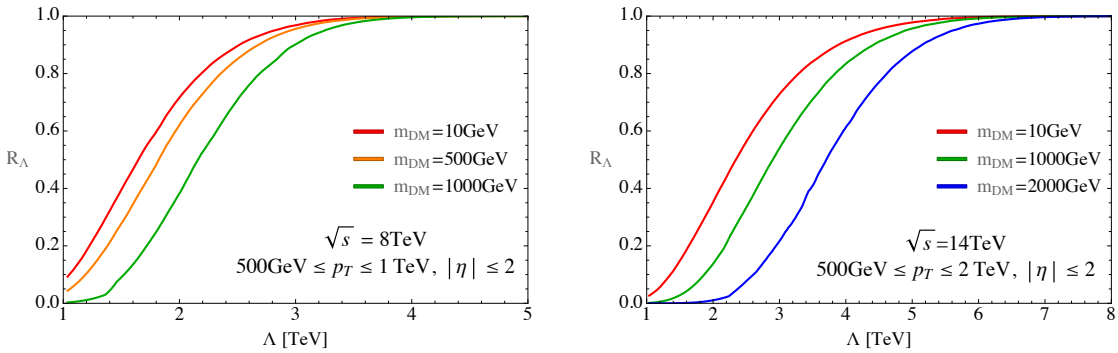

Figure 3. The ratio $R_\Lambda^{\rm tot}$ as a function of Λ for three choices of the DM mass, for $\sqrt{s} = 8\,\text{TeV}$ (left panel) and $14\,\text{TeV}$ (right panel).

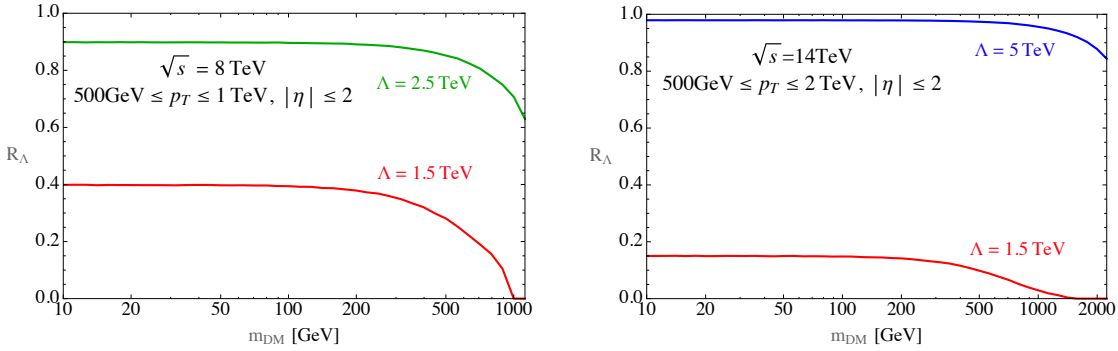

Figure 4. The ratio $R_\Lambda^{\rm tot}$ as a function of $m_{\rm DM}$ for two choices of Λ, for $\sqrt{s} = 8\,\text{TeV}$ (left panel) and $14\,\text{TeV}$ (right panel).

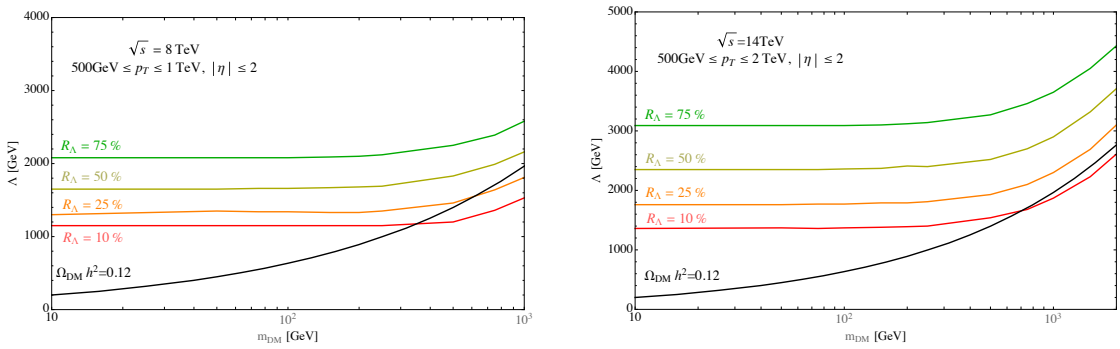

Figure 5. Contours for the ratio $R_\Lambda^{\rm tot}$, defined in eq. (2.6), on the plane $(m_{\rm DM}, \Lambda)$. We set $\sqrt{s} = 8\text{TeV}, |\eta| \leq 2$ and $500\,\text{GeV} < p_{\rm T} < 1\,\text{TeV}$ in the left panel, and $\sqrt{s} = 14\text{TeV}, |\eta| \leq 2$ and $500\,\text{GeV} < p_{\rm T} < 2\,\text{TeV}$ in the right panel. The black solid curves indicates the correct relic abundance.

JCAP09(2014)022

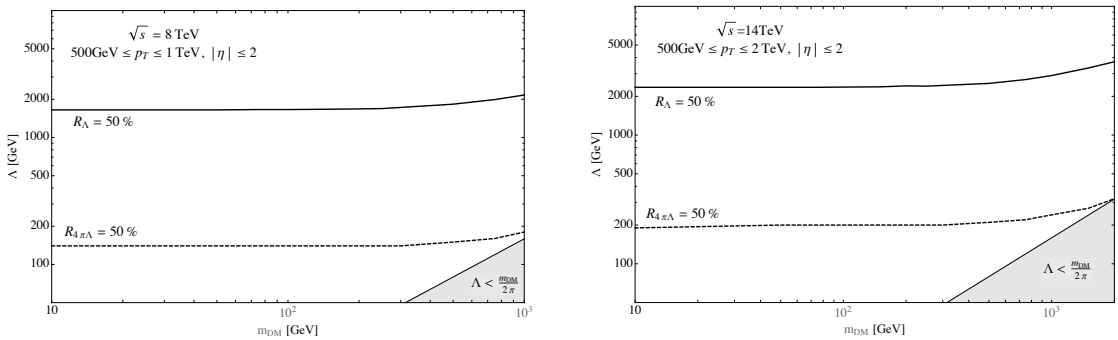

Figure 6. 50% contours for the ratio $R^{\rm tot}_\Lambda$, varying the cutoff $Q_{\rm tr} < \Lambda$ (solid line) and $Q_{\rm tr} < 4\pi\Lambda$ (dot-dashed line). We have also shown the region corresponding to $\Lambda < m_{\rm DM}/(2\pi)$ (gray shaded area), often used as a benchmark for the validity of the EFT. We set $\sqrt{s} = 8$ TeV (left panel) and $\sqrt{s} = 14$ TeV (right panel).

In figure 5 we also show the curves corresponding to the correct DM relic density, assuming that interactions between the DM particle and the SM plasma were mediated by the operator (2.1). These were computed by using a semi-analytic solution to the Boltzmann equation [38] to find the values of $m_{\rm DM}$ and Λ that yield a DM abundance matching the observed value $\Omega_{\rm DM}h^2 \simeq 0.12$ [39]. Since we are dealing with Dirac DM, have included an additional factor of 2 in the expression for the relic density relative to the equation for Majorana DM in ref. [38]. For given $m_{\rm DM}$, larger Λ leads to a smaller self-annihilation cross section and therefore to larger relic abundance. It is evident that the large-Λ region where the EFT is valid typically leads to an unacceptably large DM density. However, it may certainly be that additional annihilation channels and interactions, beyond those described by the operator (2.1) can enhance the cross section and decrease the relic abundance to fit the observations.

In the most optimistic scenario for EFTs, the coupling strength g takes the maximum value (4π) such that the model remains in the perturbative regime. In this case, a given constraint on Λ corresponds to a relatively larger value of M, such that the EFT is valid across a larger region. To demonstrate how our results depend on the coupling strength, in figure 6 we plot isocontours for $R = 50\%$, for two cases: **1)** the standard requirement that $Q^2_{\rm tr} < \Lambda^2$, equivalent to requiring $g \simeq 1$, and **2)** requiring $Q^2_{\rm tr} < (4\pi\Lambda)^2$, equivalent to requiring $g \simeq 4\pi$.

The grey shaded area indicates the region where $\Lambda < m_{\rm DM}/(2\pi)$. This is often used as a benchmark for the validity of the EFT approximation, since in the s-channel, $Q_{\rm tr}$ is kinematically forced to be greater than $2m_{\rm DM}$, leaving the EFT inherently invalid when $M < 2m_{\rm DM}$, which is equivalent to $\Lambda < m_{\rm DM}/(2\pi)$ for a coupling strength $g \simeq 4\pi$. Thus, in the s-channel the contours never cross this boundary. Interestingly this is not the case in the t-channel, since the kinematic constraints on $Q_{\rm tr}$ no longer apply. This indicates that at very large DM masses the EFT approximation can become safer than naively assumed - although in practice the ratio is still too low for EFTs to be of any practical use.

To gain a sense of whether this model is potentially observable at the LHC, and whether the effective operator model is still observable even after rescaling by R_Λ, we show in figure 7 the integrated signal cross-section at $\sqrt{s} = 14\,\text{TeV}$, using the same cuts as earlier. We can see even at relatively low dark matter masses, Λ must be smaller than $\sim$1 TeV before events

JCAP09(2014)022

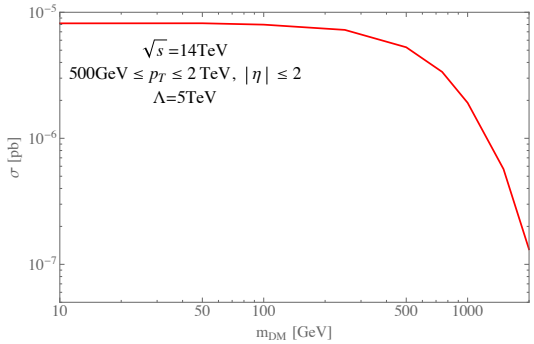

Figure 7. Cross section for the monojet process under consideration, before applying R_Λ cuts. Note that $\sigma \propto \Lambda^{-4}$.

can be expected to be produced after 25 fb^{-1}, at which point the effective operator approach has entirely ceased to be a valid approximation. At higher luminosities the model will begin to become more observable for a greater range of Λ.

2.3 Comparison with MonteCarlo simulations

As a check, it is interesting to compare our analytical results to fully numerical results. We have reproduced figure 3 using numerical simulations of the LHC events at truth level, i.e., simulating events as they would be produced in truth without simulating how they would be observed by the ATLAS or CMS detectors.

The t-channel EFT model from eq. (2.1) was constructed using FeynRules [40], and the resultant Feynman rules were exported into MadGraph 5 [41]. The process of interest, $pp \to \chi\bar{\chi}+$ jet, was simulated at a center-of-mass energy of $\sqrt{s} = 14$ TeV using the CTEQ6L1 PDF set [42]. It was found in ref. [24] that the choice of PDF influences the magnitude but not the acceptance of the rate, and therefore this different choice of PDF relative to our analytic calculations is not expected to influence the ratios we calculate. Contours in R_Λ, defined in the same way as in section 2.2, were determined by counting the fraction of events that passed the condition $Q_{\text{tr}} < \Lambda$, for both values of Q_{tr} defined in appendix A.3. Events were simulated at DM masses of 10, 50, 100, 200, 300, 500, 1000 and 2000 GeV for a wide range of values of the cutoff scale Λ. The transverse momentum and rapidity of the jet are restricted to the ranges $(500 \leq p_{\text{T}}/\text{GeV} \leq 2000)$ and $|\eta| \leq 2$ respectively, as in the analytic results from the previous section.

3 Conclusions

In this paper we have extended the investigation of the validity of the EFT approach for DM searches at the LHC. While in refs. [23, 24] our analysis has been focused on the case of the EFT operators generated by integrating out a heavy mediator in the s-channel, we have considered here the case of Dirac DM couplings to the standard model via the t-channel. Even though a t-channel operator can be expressed by a Fierz transformation as a sum of s-channel operators, our results as a function of Λ and DM mass (compared, for instance, to those of figure 2 of ref. [24]) indicate that one may not infer them from those of a single s-channel operator, see eq. (2.4). This is due to the inherently different kinematics of the s- and t-channel, in particular significant differences in the transferred momentum.

JCAP09(2014)022

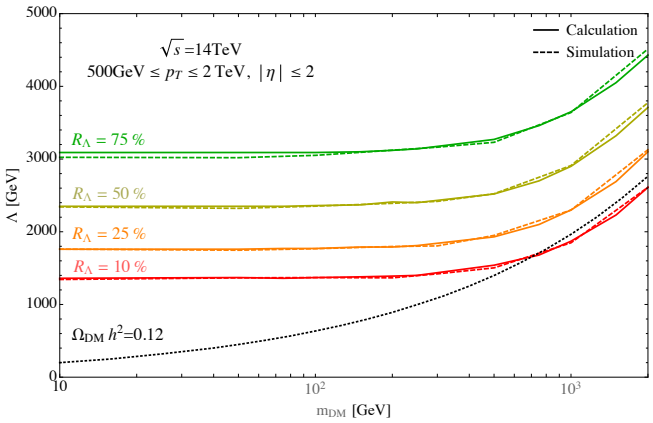

Figure 8. Comparison of the contour $R_\Lambda^{\rm tot} = 50\%$ for the analytical calculation (solid line) and the simulation (dashed line). The dotted curve indicates the correct relic abundance.

We have also computed the relic density over the parameter space of the model, assuming that the only interactions between DM and the SM are those mediated by the t-channel operator (2.1), and found that the region of EFT validity corresponds to an overly large relic density. This conclusion is rather general and may be evaded by assuming additional DM annihilation channels.

Similar to what happens in the s-channel case, our findings indicate that in the t-channel the range of validity of the EFT is significantly limited in the parameter space $(\Lambda, m_{\rm DM})$, reinforcing the need to go beyond the EFT at the LHC when looking for DM signals. This is especially true for light mediators as they can be singly produced in association with a DM particle, leading to a qualitatively new contribution to the mono-jet processes. Mediators can even be pair-produced at the LHC through both QCD processes and DM exchange processes. All of this rich dynamics leads to stronger signals (and therefore, in the absence thereof, to tighter bounds) than the EFT approach.

Acknowledgments

We thank A. Brennan, C. Doglioni, G. Iacobucci, S. Schramm and S. Vallecorsa for many interesting conversations. ADS acknowledges partial support from the European Union FP7 ITN INVISIBLES (Marie Curie Actions, PITN-GA-2011-289442).

A Three-body cross sections

In this appendix we show the details of the calculations of the tree-level cross sections for the hard scattering processes $q(p_1) + \bar{q}(p_2) \to \chi(p_3) + \chi(p_4) + g(k)$ and $q(p_1) + g(p_2) \to \chi(p_3) + \chi(p_4) + q(k)$, computed using the effective Lagrangian of eq. (2.1).

JCAP09(2014)022

A.1 Matrix elements

The amplitudes for the process we are interested in are described, at leading order, by the Feyman diagrams in figure 1. In the EFT limit they are given by

$$\begin{aligned}
\mathcal{M}_g &= -i\,\frac{g^2 g_s}{M^2}\epsilon^*_\mu T^a_{ij} \times \\
&\quad \times \left\{ \frac{\bar{u}(p_3)P_L(\not{p}_1 - \not{p}_2)\gamma^\mu u(p_1)\bar{v}(p_2)P_R v(p_4)}{(p_1-k)^2} - \frac{\bar{u}(p_3)P_L u(p_1)\bar{v}(p_2)P_R\gamma^\mu(\not{p}_2 - \not{k})v(p_4)}{(p_2-k)^2} \right\} \\
\mathcal{M}_q &= -i\,\frac{g^2 g_s}{M^2}\epsilon_\mu T^a_{ij} \times \\
&\quad \times \left\{ \frac{\bar{u}(k)P_R v(p_3)\bar{u}(p_4)P_L(\not{p}_1 + \not{p}_2)\gamma^\mu u(p_1)}{(p_1+p_2)^2} - \frac{\bar{u}(k)\gamma^\mu(\not{p}_2 - \not{k})P_R v(p_3)\bar{u}(p_4)P_L u(p_1)}{(p_2-k)^2} \right\} \\
\mathcal{M}_{\bar{q}} &= -i\,\frac{g^2 g_s}{M^2}\epsilon_\mu T^a_{ij} \times \\
&\quad \times \left\{ \frac{\bar{v}(k)P_L u(p_3)\bar{v}(p_4)P_R(\not{p}_1 + \not{p}_2)\gamma^\mu v(p_1)}{(p_1+p_2)^2} - \frac{\bar{v}(k)\gamma^\mu(\not{p}_2 - \not{k})P_L u(p_3)\bar{v}(p_4)P_R v(p_1)}{(p_2-k)^2} \right\}
\end{aligned} \tag{A.1}$$

for the gluon, quark and anti-quark emission processes respectively. Here we denote the gluon polarization vector by ϵ_μ and the left and right projectors $(1-\gamma_5)/2$ and $(1+\gamma_5)/2$ with P_L and P_R respectively. The matrix T^a_{ij} stands for the standard QCD Gell-Mann matrices. Notice that we work in the massless quark limit. The anti-quark matrix element is simply obtained from the quark one by exchanging quarks with anti-quarks and left with right projectors. The parton level cross sections for the two processes are thus the same, so here we only show the explicit derivation of the quark one. The squared amplitudes, averaged over initial states (spin and colour) and summed over the final states, are given by

$$\begin{aligned}
|\mathcal{M}_g|^2 &= \frac{1}{9}\frac{g_s^2}{\Lambda^4}\frac{1}{(k\cdot p_1)(k\cdot p_2)} \times \\
&\quad \Big\{ p_1\cdot p_3 \Big[(k\cdot p_4)(k\cdot p_1) - (k\cdot p_4)(p_1\cdot p_2) - (k\cdot p_2)(p_1\cdot p_4) \Big] + \\
&\quad + p_2\cdot p_4 \Big[(k\cdot p_3)(k\cdot p_2) - (k\cdot p_3)(p_1\cdot p_2) - (k\cdot p_1)(p_2\cdot p_3) \Big] + \\
&\quad + (p_1\cdot p_3)(p_2\cdot p_4)\Big[2p_1\cdot p_2 - k\cdot p_1 - k\cdot p_2 \Big] \Big\}
\end{aligned} \tag{A.2}$$

$$\begin{aligned}
|\mathcal{M}_q|^2 &= \frac{1}{6}\frac{g_s^2}{\Lambda^4}\frac{1}{(k\cdot p_1)(k\cdot p_2)} \times \\
&\quad \Big\{ p_1\cdot p_4 \Big[(k\cdot p_2)(p_1\cdot p_3) - (k\cdot p_1)(p_2\cdot p_3) + \\
&\quad + (k\cdot p_2)(k\cdot p_3) + (k\cdot p_1)(k\cdot p_3) - (p_1\cdot p_2)(k\cdot p_3) \Big] + \\
&\quad + p_2\cdot p_2 \Big[(p_1\cdot p_4)(p_2\cdot p_3) - (k\cdot p_4)(k\cdot p_3) \Big] + \\
&\quad + (k\cdot p_3)\Big[(k\cdot p_1)(p_1\cdot p_4) + (k\cdot p_1)(p_2\cdot p_4) + (k\cdot p_2)(p_2\cdot p_4) \Big] \Big\}
\end{aligned} \tag{A.3}$$

with $\Lambda^2 = M^2/g^2$.

JCAP09(2014)022

A.2 Cross sections

The simplest way to compute the cross section in the lab frame is to first evaluate the matrix elements and the phase space density in the center-of-mass (c.o.m.) frame, and then boost the result to the lab frame. In the c.o.m. frame, let us parametrize the four-momenta inolved in the process as

$$p_1 = x\frac{\sqrt{s}}{2}(1,0,0,1)\,, \qquad p_2 = x\frac{\sqrt{s}}{2}(1,0,0,-1)\,, \qquad k = x\frac{\sqrt{s}}{2}\left(z_0, z_0\hat{k}\right)\,, \tag{A.4}$$
$$p_3 = x\frac{\sqrt{s}}{2}\left(1-y_0, \sqrt{(1-y_0)^2-a^2}\hat{p}_3\right), \quad p_4 = x\frac{\sqrt{s}}{2}\left(1+y_0-z_0, \sqrt{(1+y_0-z_0)^2-a^2}\hat{p}_4\right),$$

where the two colliding partons carry equal momentum fractions $x_1 = x_2 \equiv x$ of the incoming protons, $a \equiv 2m_{\rm DM}/(x\sqrt{s}) < 1$, $\hat{k} = (0, \sin\theta_0, \cos\theta_0)$, and θ_0 is the polar angle of $\hat{k}$ with respect to the beam line, in the c.o.m. frame. The subscript $_0$ denotes quantities evaluated in the c.o.m. frame.

The differential cross section is generically given by

$$d\hat{\sigma} = \frac{\sum\overline{|\mathcal{M}|^2}}{4(p_1\cdot p_2)}\mathrm{d}\Phi_3\,, \tag{A.5}$$

where the three-body phase space is

$$\mathrm{d}\Phi_3 = (2\pi)^4\delta(E_1+E_2-E_3-E_4-E_k)\,\delta^{(3)}\left(\vec{p}_1+\vec{p}_2-\vec{p}_3-\vec{p}_4-\vec{k}\right)\frac{\mathrm{d}^3p_3}{(2\pi)^3 2E_3}\frac{\mathrm{d}^3p_4}{(2\pi)^3 2E_4}\frac{\mathrm{d}^3k}{(2\pi)^3 2E_k}. \tag{A.6}$$

Using the three-momentum delta function, we can integrate away d^3p_4; the energy delta function instead fixes the angle $\theta_{0\,3\mathrm{j}}$ between $\hat{p}_3$ and the jet $\hat{k}$ as: $\cos\theta_{0\,3\mathrm{j}} = (\mathbf{p}_4^2 - \mathbf{k}^2 - \mathbf{p}_3^2)/2|\mathbf{k}||\mathbf{p}_3|$. Integration over the azimuthal angle ϕ_0 of the outgoing jet simply gives a factor of 2π, while the matrix element does depend on the azimuthal angle of the three-momentum $\vec{p}_3$ with respect to $\vec{k}$, $\phi_{0\,3\mathrm{j}}$, and so it can not be integrated over at this stage, contrary to the s-channel case. Taking all of this into account, the phase space density simplifies to

$$\mathrm{d}\Phi_3 = \frac{1}{8(2\pi)^4}\,\mathrm{d}E_3\,\mathrm{d}|\vec{k}|\,\mathrm{d}\cos\theta_0\,\mathrm{d}\phi_{0\,3\mathrm{j}} = \frac{x^2 s}{32(2\pi)^4}\,\mathrm{d}y_0\,\mathrm{d}z_0\,\mathrm{d}\cos\theta_0\,\mathrm{d}\phi_{0\,3\mathrm{j}}. \tag{A.7}$$

The kinematical domains of y_0, z_0 and $\phi_{0\,3\mathrm{j}}$ are

$$\frac{z_0}{2}\left(1-\sqrt{\frac{1-z_0-a^2}{1-z_0}}\right) \le \; y_0 \; \le \frac{z_0}{2}\left(1+\sqrt{\frac{1-z_0-a^2}{1-z_0}}\right) \tag{A.8}$$
$$0 \le \; z_0 \; \le 1-a^2 \tag{A.9}$$
$$0 \le \phi_{0\,3\mathrm{j}} \le 2\pi \tag{A.10}$$

The variables y_0 and $\phi_{0\,3\mathrm{j}}$ refer to the momentum $\vec{p}_3$ of an invisible DM particle; they are therefore not measurable, and we integrate over them. For our present purpose, finding the total integrated cross section is useless, since these variables enter our definition of the momentum transfer $Q_{\rm tr}$, and the condition $Q_{\rm tr} < \Lambda$ which we used to define the ratio R_Λ.

JCAP09(2014)022

With the matrix elements of eqs. (A.2) and (A.3), and the phase space density A.7, we get the differential cross sections in the c.o.m. frame:

$$\left.\frac{\mathrm{d}^4\hat{\sigma}}{\mathrm{d}z_0\,\mathrm{d}\cos\theta_0\,\mathrm{d}y_0\,\mathrm{d}\phi_{0\,3\mathrm{j}}}\right|_g = \frac{1}{4608\pi^4}\frac{g_s^2}{\Lambda^4}\frac{1-z_0}{z_0^4}$$
$$\Bigg\{4x(2-z_0)\csc\theta_0\cos\phi_{0\,3\mathrm{j}}(\cos\theta_0(z_0-2y_0)+z_0)\sqrt{s\left(sx^2y_0(z_0-1)(y_0-z_0)-m_{\mathrm{DM}}^2z_0^2\right)}$$
$$-8m_{\mathrm{DM}}^2z_0^2\cos^2\phi_{0\,3\mathrm{j}}+sx^2((z_0-2)z_0+2)\left(\sec^2(\theta_0/2)\,y_0^2+\csc^2(\theta_0/2)\,(y_0-z_0)^2\right)$$
$$-2sx^2y_0^2((z_0-6)z_0+6)+4sx^2y_0(z_0-1)(y_0-z_0)\cos(2\phi_{0\,3\mathrm{j}})$$
$$+2sx^2y_0((z_0-6)z_0+6)z_0-sx^2z_0^2((z_0-2)z_0+2)\Bigg\}, \tag{A.11}$$

$$\left.\frac{\mathrm{d}^4\hat{\sigma}}{\mathrm{d}z_0\,\mathrm{d}\cos\theta_0\,\mathrm{d}y_0\,\mathrm{d}\phi_{0\,3\mathrm{j}}}\right|_q = \frac{1}{98304\pi^4}\frac{g_s^2}{\Lambda^4}\frac{1-z_0}{z_0^3\cos^2\frac{\theta_0}{2}}$$
$$\Bigg\{8x\sqrt{s}\left[z_0(z_0-y_0-1)-\left(z_0^2-(1+y_0)z_0+2y_0\right)\cos\theta_0\right]\cos\phi_{0\,3\mathrm{j}}\sin\theta_0\times$$
$$\times\sqrt{sx^2y_0(z_0-y_0)(1-z_0)-m_{\mathrm{DM}}^2z_0^2}$$
$$-2(1-\cos(2\theta_0))m_{\mathrm{DM}}^2z_0^2+4\Big[sx^2y_0(z_0-y_0)(1-z_0)-m_{\mathrm{DM}}^2z_0^2\Big]\cos(2\phi_{0\,3\mathrm{j}})\sin^2\theta_0$$
$$+sx^2\Big[11z_0^4-(6+22y_0)z_0^3+(11y_0^2+8y_0+3)z_0^2-2y_0(1+y_0)z_0+2y_0^2\Big]$$
$$+sx^2\Big[z_0^4-2(1+y_0)z_0^3+(y_0^2+8y_0+1)z_0^2-6y_0(1+y_0)z_0+6y_0^2\Big]\cos(2\theta_0)$$
$$-4sx^2z_0\Big[z_0^3-2(1+y_0)z_0^2+(y_0^2+4y_0+1)z_0-2y_0(1+y_0)\Big]\cos\theta_0\Bigg\}. \tag{A.12}$$

To get the cross sections in the lab frame we perform a boost in the $\hat{z}$ axis, accounting for the generic parton momentum fractions x_1, x_2. The velocity of the c.o.m. of the colliding particles with respect to the lab frame is given by

$$\beta_{\mathrm{c.o.m.}} = \frac{x_1-x_2}{x_1+x_2}, \tag{A.13}$$

so that the relations between the quantities z_0, θ_0 and the analogous ones z, θ in the lab frame are

$$\begin{aligned} z_0 &= \frac{(x_1+x_2)^2+\left(x_2^2-x_1^2\right)\cos\theta}{4x_1x_2}z \\ \sin^2\theta_0 &= \frac{4x_1x_2}{[(x_1+x_2)+(x_2-x_1)\cos\theta]^2}\sin^2\theta. \end{aligned} \tag{A.14}$$

JCAP09(2014)022

The Jacobian factor to transform $\mathrm{d}z_0\,\mathrm{d}\cos\theta_0 \to \mathrm{d}z\,\mathrm{d}\cos\theta$ is simply obtained using equations (A.14); the cross section in the lab frame is then

$$\frac{\mathrm{d}^4\hat{\sigma}}{\mathrm{d}z\,\mathrm{d}\cos\theta\,\mathrm{d}y_0\,\mathrm{d}\phi_{0\,3\mathrm{j}}} = \frac{x_1+x_2}{x_1+x_2+(x_1-x_2)\cos\theta}\,\frac{\mathrm{d}^4\hat{\sigma}}{\mathrm{d}z_0\,\mathrm{d}\cos\theta_0\,\mathrm{d}y_0\,\mathrm{d}\phi_{0\,3\mathrm{j}}}\bigg|_{\substack{z_0\to z_0(z)\\ \theta_0\to\theta_0(\theta)}} . \tag{A.15}$$

Expressing the energy of the emitted gluon or (anti-)quark in terms of the transverse momentum and rapidity, $k^0 = p_\mathrm{T}\cosh\eta$, one finds

$$z = \frac{4p_\mathrm{T}\cosh\eta}{(x_1+x_2)\sqrt{s}}, \qquad \cos\theta = \tanh\eta \tag{A.16}$$

which allows us to express the differential cross sections with respect to the transverse momentum and pseudo-rapidity of the emitted jet:

$$\frac{\mathrm{d}^4\hat{\sigma}}{\mathrm{d}p_\mathrm{T}\,\mathrm{d}\eta\,\mathrm{d}y_0\,\mathrm{d}\phi_{0\,3\mathrm{j}}} = \frac{4}{(x_1+x_2)\sqrt{s}\cosh\eta}\,\frac{\mathrm{d}^4\hat{\sigma}}{\mathrm{d}z\,\mathrm{d}\cos\theta\,\mathrm{d}y_0\,\mathrm{d}\phi_{0\,3\mathrm{j}}}\bigg|_{\substack{z\to z(p_\mathrm{T},\eta)\\ \theta\to\theta(p_\mathrm{T},\eta)}} . \tag{A.17}$$

A.3 Transferred momentum

As is clear from our arguments, the key ingredient to quantify the validity of the EFT approximation is the value of the transferred momentum of the process. Since each process of interest here is given (at tree level) by the contribution of two Feynman diagrams, there will also be two expressions for the transferred momentum for both gluon and (anti-)quark emission, which we report here:

$$\begin{aligned}
Q^2_{\mathrm{tr,g1}} &= (p_1-k-p_3)^2 \\
&= m^2_\mathrm{DM} + \sqrt{s}x_2e^\eta p_\mathrm{T} - \frac{e^{2\eta}(1+y)\left(x_1x_2^2s\right)}{x_1+e^{2\eta}x_2} - \frac{x_1^2x_2^2e^\eta s^{3/2}y\left(x_1-e^{2\eta}x_2\right)}{p_\mathrm{T}\left(x_1+e^{2\eta}x_2\right)^2} \\
&\quad -\frac{2e^\eta x_1x_2\sqrt{s}\cos\phi_{0\,3\mathrm{j}}}{p_\mathrm{T}(x_1+e^{2\eta}x_2)^2}\Big[-m^2_\mathrm{DM}p_\mathrm{T}^2\left(x_1+e^{2\eta}x_2\right)^2 \\
&\quad -sx_1x_2y\left(e^\eta\sqrt{s}x_1x_2-p_\mathrm{T}\left(x_1+e^{2\eta}x_2\right)\right)\left(e^\eta\sqrt{s}x_1x_2y-p_\mathrm{T}\left(x_1+e^{2\eta}x_2\right)\right)\Big]^{1/2}\Bigg\},
\end{aligned} \tag{A.18}$$

$$\begin{aligned}
Q^2_{\mathrm{tr,g2}} &= (p_1-p_3)^2 \\
&= m^2_\mathrm{DM} + \frac{x_1x_2s(x_1-e^{2\eta}x_2)}{x_1+e^{2\eta}x_2} - \frac{(1-y)\left(x_1^2x_2s\right)}{x_1+e^{2\eta}x_2} - \frac{x_1^2x_2^2e^\eta s^{3/2}y(x_1-e^{2\eta}x_2)}{p_\mathrm{T}\left(x_1+e^{2\eta}x_2\right)^2} \\
&\quad -\frac{2e^\eta x_1x_2\sqrt{s}\cos\phi_{0\,3\mathrm{j}}}{p_\mathrm{T}(x_1+e^{2\eta}x_2)^2}\Big[-m^2_\mathrm{DM}p_\mathrm{T}^2\left(x_1+e^{2\eta}x_2\right)^2 \\
&\quad -sx_1x_2y\left(e^\eta\sqrt{s}x_1x_2-p_\mathrm{T}\left(x_1+e^{2\eta}x_2\right)\right)\left(e^\eta\sqrt{s}x_1x_2y-p_\mathrm{T}\left(x_1+e^{2\eta}x_2\right)\right)\Big]^{1/2}\Bigg\},
\end{aligned} \tag{A.19}$$

$$\begin{aligned}
Q^2_{\mathrm{tr,q1}} &= (p_3+k)^2 \\
&= m^2_\mathrm{DM} + p_\mathrm{T}\sqrt{s}\left(e^{-\eta}x_1+e^\eta x_2\right) - x_1x_2s\,y,
\end{aligned} \tag{A.20}$$

JCAP09(2014)022

$$
\begin{aligned}
Q^2_{\mathrm{tr,q2}} &= (p_1 - p_3 - k)^2 \\
&= m^2_{\mathrm{DM}} + \sqrt{s} x_1 e^{-\eta} p_{\mathrm{T}} - \frac{(1+y)\left(x_1^2 x_2 s\right)}{x_1 + e^{2\eta} x_2} + \frac{x_1^2 x_2^2 e^{\eta} s^{3/2} y (x_1 - e^{2\eta} x_2)}{p_{\mathrm{T}} (x_1 + e^{2\eta} x_2)^2} \\
&\quad - \frac{2 e^{\eta} x_1 x_2 \sqrt{s} \cos\phi_{0\,3\mathrm{j}}}{p_{\mathrm{T}} (x_1 + e^{2\eta} x_2)^2} \Big[-m^2_{\mathrm{DM}} p^2_{\mathrm{T}} \left(x_1 + e^{2\eta} x_2\right)^2 \\
&\quad - s x_1 x_2 y \left(e^{\eta} \sqrt{s} x_1 x_2 - p_{\mathrm{T}} \left(x_1 + e^{2\eta} x_2\right)\right) \left(e^{\eta} \sqrt{s} x_1 x_2 y - p_{\mathrm{T}} \left(x_1 + e^{2\eta} x_2\right)\right) \Big]^{1/2}.
\end{aligned}
\tag{A.21}
$$

The notation g, q stands for gluon or quark emission; the indices $1, 2$ refer to emission from each of the initial state particles.

References

[1] L. Baudis, *Direct dark matter detection: the next decade*, *Phys. Dark Univ.* **1** (2012) 94 [arXiv:1211.7222] [INSPIRE].

[2] M. Cirelli, *Indirect Searches for Dark Matter: a status review*, *Pramana* **79** (2012) 1021 [arXiv:1202.1454] [INSPIRE].

[3] J.L. Feng, S. Ritz, J.J. Beatty, J. Buckley, D.F. Cowen et al., *Planning the Future of U.S. Particle Physics (Snowmass 2013): Chapter 4: Cosmic Frontier*, arXiv:1401.6085 [INSPIRE].

[4] H.E.S.S.Collaboration collaboration, A. Abramowski et al., *Search for a Dark Matter annihilation signal from the Galactic Center halo with H.E.S.S*, *Phys. Rev. Lett.* **106** (2011) 161301 [arXiv:1103.3266] [INSPIRE].

[5] Fermi-LAT collaboration, M. Ackermann et al., *Dark Matter Constraints from Observations of 25 Milky Way Satellite Galaxies with the Fermi Large Area Telescope*, *Phys. Rev.* **D 89** (2014) 042001 [arXiv:1310.0828] [INSPIRE].

[6] XENON100 collaboration, E. Aprile et al., *Dark Matter Results from 225 Live Days of XENON100 Data*, *Phys. Rev. Lett.* **109** (2012) 181301 [arXiv:1207.5988] [INSPIRE].

[7] LUX collaboration, D.S. Akerib et al., *First results from the LUX dark matter experiment at the Sanford Underground Research Facility*, *Phys. Rev. Lett.* **112** (2014) 091303 [arXiv:1310.8214] [INSPIRE].

[8] DAMA Collaboration, LIBRA collaboration, R. Bernabei et al., *New results from DAMA/LIBRA*, *Eur. Phys. J.* **C 67** (2010) 39 [arXiv:1002.1028] [INSPIRE].

[9] CDMS collaboration, R. Agnese et al., *Silicon Detector Dark Matter Results from the Final Exposure of CDMS II*, *Phys. Rev. Lett.* **111** (2013) 251301 [arXiv:1304.4279] [INSPIRE].

[10] CoGeNT collaboration, C.E. Aalseth et al., *CoGeNT: A Search for Low-Mass Dark Matter using p-type Point Contact Germanium Detectors*, *Phys. Rev.* **D 88** (2013) 012002 [arXiv:1208.5737] [INSPIRE].

[11] ATLAS collaboration, *Search for dark matter candidates and large extra dimensions in events with a jet and missing transverse momentum with the ATLAS detector*, *JHEP* **04** (2013) 075 [arXiv:1210.4491] [INSPIRE].

[12] CMS collaboration, *Search for New Physics with a Mono-Jet and Missing Transverse Energy in pp Collisions at $\sqrt{s} = 7$ TeV*, *Phys. Rev. Lett.* **107** (2011) 201804 [arXiv:1106.4775] [INSPIRE].

[13] ATLAS collaboration, *Search for New Phenomena in Monojet plus Missing Transverse Momentum Final States using 10fb-1 of pp Collisions at $\sqrt{s} = 8\,TeV$ with the ATLAS detector at the LHC*, ATLAS-CONF-2012-147 (2012) [INSPIRE].

JCAP09(2014)022

[14] CMS collaboration, *Search for new physics in monojet events in pp collisions at* $\sqrt{s} = 8\,TeV$, CMS-PAS-EXO-12-048 (2013) [INSPIRE].

[15] ATLAS collaboration, *Search for dark matter pair production in events with a hadronically decaying W or Z boson and missing transverse momentum in pp collision data at* $\sqrt{s} = 8\,TeV$ *with the ATLAS detector*, ATLAS-CONF-2013-073 (2013) [INSPIRE].

[16] ATLAS collaboration, *Search for dark matter in events with a Z boson and missing transverse momentum in pp collisions at* $\sqrt{s}$*=8 TeV with the ATLAS detector*, *Phys. Rev.* **D 90** (2014) 012004 [arXiv:1404.0051] [INSPIRE].

[17] ATLAS collaboration, *Search for dark matter candidates and large extra dimensions in events with a photon and missing transverse momentum in pp collision data at* $\sqrt{s} = 7$ *TeV with the ATLAS detector*, *Phys. Rev. Lett.* **110** (2013) 011802 [arXiv:1209.4625] [INSPIRE].

[18] CMS collaboration, *Search for Dark Matter and Large Extra Dimensions in pp Collisions Yielding a Photon and Missing Transverse Energy*, *Phys. Rev. Lett.* **108** (2012) 261803 [arXiv:1204.0821] [INSPIRE].

[19] ATLAS collaboration, *Search for dark matter candidates and large extra dimensions in events with a photon and missing transverse momentum in pp collision data at* $\sqrt{s} = 7\,TeV$ *with the ATLAS detector*, ATLAS-CONF-2012-085 (2012) [INSPIRE].

[20] CMS collaboration, *Search for ADD Extra-dimensions in Monophotons*, CMS-PAS-EXO-11-058 (2011) [INSPIRE].

[21] A. De Simone, G.F. Giudice and A. Strumia, *Benchmarks for Dark Matter Searches at the LHC*, *JHEP* **06** (2014) 081 [arXiv:1402.6287] [INSPIRE].

[22] A. Alves, S. Profumo and F.S. Queiroz, *The dark* $Z^{'}$ *portal: direct, indirect and collider searches*, *JHEP* **04** (2014) 063 [arXiv:1312.5281] [INSPIRE].

[23] G. Busoni, A. De Simone, E. Morgante and A. Riotto, *On the Validity of the Effective Field Theory for Dark Matter Searches at the LHC*, *Phys. Lett.* **B 728** (2014) 412 [arXiv:1307.2253] [INSPIRE].

[24] G. Busoni, A. De Simone, J. Gramling, E. Morgante and A. Riotto, *On the Validity of the Effective Field Theory for Dark Matter Searches at the LHC, Part II: Complete Analysis for the s-channel*, *JCAP* **06** (2014) 060 [arXiv:1402.1275] [INSPIRE].

[25] P.J. Fox, R. Harnik, J. Kopp and Y. Tsai, *Missing Energy Signatures of Dark Matter at the LHC*, *Phys. Rev.* **D 85** (2012) 056011 [arXiv:1109.4398] [INSPIRE].

[26] O. Buchmueller, M.J. Dolan and C. McCabe, *Beyond Effective Field Theory for Dark Matter Searches at the LHC*, *JHEP* **01** (2014) 025 [arXiv:1308.6799] [INSPIRE].

[27] N.F. Bell, J.B. Dent, A.J. Galea, T.D. Jacques, L.M. Krauss et al., *Searching for Dark Matter at the LHC with a Mono-Z*, *Phys. Rev.* **D 86** (2012) 096011 [arXiv:1209.0231] [INSPIRE].

[28] S. Chang, R. Edezhath, J. Hutchinson and M. Luty, *Effective WIMPs*, *Phys. Rev.* **D 89** (2014) 015011 [arXiv:1307.8120] [INSPIRE].

[29] H. An, L.-T. Wang and H. Zhang, *Dark matter with t-channel mediator: a simple step beyond contact interaction*, *Phys. Rev.* **D 89** (2014) 115014 [arXiv:1308.0592] [INSPIRE].

[30] Y. Bai and J. Berger, *Fermion Portal Dark Matter*, *JHEP* **11** (2013) 171 [arXiv:1308.0612] [INSPIRE].

[31] A. DiFranzo, K.I. Nagao, A. Rajaraman and T.M.P. Tait, *Simplified Models for Dark Matter Interacting with Quarks*, *JHEP* **11** (2013) 014 [arXiv:1308.2679] [INSPIRE].

[32] M. Papucci, A. Vichi and K.M. Zurek, *Monojet versus rest of the world I: t-channel Models*, arXiv:1402.2285 [INSPIRE].

JCAP09(2014)022

[33] M. Garny, A. Ibarra, S. Rydbeck and S. Vogl, *Majorana Dark Matter with a Coloured Mediator: Collider vs Direct and Indirect Searches*, *JHEP* **06** (2014) 169 [arXiv:1403.4634] [INSPIRE].

[34] N.F. Bell, J.B. Dent, T.D. Jacques and T.J. Weiler, *W/Z Bremsstrahlung as the Dominant Annihilation Channel for Dark Matter*, *Phys. Rev.* **D 83** (2011) 013001 [arXiv:1009.2584] [INSPIRE].

[35] J. Goodman, M. Ibe, A. Rajaraman, W. Shepherd, T.M.P. Tait et al., *Constraints on Dark Matter from Colliders*, *Phys. Rev.* **D 82** (2010) 116010 [arXiv:1008.1783] [INSPIRE].

[36] A.D. Martin, W.J. Stirling, R.S. Thorne and G. Watt, *Parton distributions for the LHC*, *Eur. Phys. J.* **C 63** (2009) 189 [arXiv:0901.0002] [INSPIRE].

[37] http://mstwpdf.hepforge.org/.

[38] G. Bertone, D. Hooper and J. Silk, *Particle dark matter: Evidence, candidates and constraints*, *Phys. Rept.* **405** (2005) 279 [hep-ph/0404175] [INSPIRE].

[39] PLANCK collaboration, P.A.R. Ade et al., *Planck 2013 results. XVI. Cosmological parameters*, *Astron. Astrophys.* (2014) [arXiv:1303.5076] [INSPIRE].

[40] N.D. Christensen and C. Duhr, *FeynRules - Feynman rules made easy*, *Comput. Phys. Commun.* **180** (2009) 1614 [arXiv:0806.4194] [INSPIRE].

[41] J. Alwall, M. Herquet, F. Maltoni, O. Mattelaer and T. Stelzer, *MadGraph 5 : Going Beyond*, *JHEP* **06** (2011) 128 [arXiv:1106.0522] [INSPIRE].

[42] J. Pumplin, D.R. Stump, J. Huston, H.L. Lai, P.M. Nadolsky et al., *New generation of parton distributions with uncertainties from global QCD analysis*, *JHEP* **07** (2002) 012 [hep-ph/0201195] [INSPIRE].

JCAP09(2014)022